Applied Radiation and Isotopes 116 (2016) 1–7

Contents lists available at ScienceDirect

Applied Radiation and Isotopes

journal homepage: www.elsevier.com/locate/apradiso

Performance of ZnSe(Te) as fiberoptic dosimetry detector

M. Ramírez [a,b], N. Martínez [a], J. Marcazzó [a,*], P. Molina [a], D. Feld [c], M. Santiago [a]

[a] Instituto de Física Arroyo Seco (UNCPBA) and CIFICEN (UNCPBA – CICPBA – CONICET), Pinto 399, 7000 Tandil, Argentina
[b] Facultad de Ciencias Exactas y Aplicadas, Instituto Tecnológico Metropolitano (ITM), Calle 73 No 76 A 354, Medellín, Colombia
[c] Instituto de Oncología Ángel H. Roffo, Av. San Martín, CABA, 5481 Argentina

HIGHLIGHTS

- Red-emitting ZnSe(Te) scintillator as fiberoptic dosimetry detector is investigated.
- Stems effect can be efficiently reduced by optical filtering.
- ZnSe(Te)-based dosimetry probes are suitable for small-field dosimetry in LINAC.

ARTICLE INFO

Article history:
Received 10 December 2015
Received in revised form
29 June 2016
Accepted 10 July 2016
Available online 11 July 2016

Keywords:
Fiber optic dosimetry
Real time dosimetry
Tellurium doped zinc selenide
ZnSe(Te)

ABSTRACT

Fiberoptic dosimetry (FOD) is an experimental technique suitable for in-vivo, real time dosimetry in radiotherapy treatments. FOD relies on using a small scintillator coupled to one end of a long optical fiber. The scintillator is placed at the point where the dose rate is to be determined whereas a light detector at the other end of the fiber measures the intensity of the radioluminescence emitted by the scintillator. One of the problems hampering the straightforward application of this technique in clinics is the presence of Cherenkov radiation generated in the fiber by the ionizing radiation, which adds to the scintillating light and introduces a bias in the dose measurement. Since Cherenkov radiation is more important in short wavelength range of the visible spectrum, using red-emitting scintillators as FOD detectors permits to reduce the Cherenkov contribution by using optical filters. In this work, the performance of red-emitting tellurium-doped zinc selenide crystal as FOD detector is evaluated and compared to the response of an ion-chamber.

1. Introduction

The most recent techniques for radiation treatment of cancer such as stereotactic radiotherapy, intensity-modulated radiation therapy and Cyberknife™, have as their main goal to conform the delivered dose more tightly to the tumor and to prevent critical organs from being unnecessarily irradiated. These techniques, which are characterized by small fields and high dose gradients, require real time high resolution dosimetry systems to verify that the planned dose distributions corresponds to the doses delivered clinically to the patient (Lambert et al., 2010). Real time dosimetry is also recommended in high-dose brachytherapy treatments, where planned dose distributions might differ from the clinically delivered doses (Seymour et al., 2011; Caraca Santos et al., 2015). In this context, the experimental dosimetry technique known as fiberoptic dosimetry (FOD) has become an attractive alternative to traditional dosimetry systems due to the small size of the radiation detectors employed (Beddar et al., 1992a; Létourneau et al., 1999; Huston et al., 2001; Polf et al., 2004; Beierholm et al., 2011, 2012).

FOD relies on using a small piece of scintillator ($\approx 1\ mm^3$) attached to the end of an optical fiber, which guides the light emitted by the scintillator during irradiation outside the treatment room up to a light detector. In general, the intensity of the scintillating light or radioluminescence (RL) can be regarded as proportional to the dose rate absorbed by the scintillator (Aznar et al., 2004; Teichmann et al., 2016). FOD presents very attractive features: (a) the small detector size maximizes spatial resolution compared to other types of detectors; (b) it is not necessary to apply an electric potential to the detector; (c) it is a robust system which can endure the routine clinical use; and, (d) it allows real time measurements (Justus et al., 2004).

A shortcoming affecting FOD comes from the intrinsic light emission induced by ionizing radiation in the optical fiber, which adds to the scintillator light yield. The main components of this light, usually called stem effect, has two origins: the own optical fiber fluorescence and the luminescence due to Cherenkov effect (Beddar et al., 1992a). In the PMMA (polymethylmethacrylate)

* Corresponding author.

http://dx.doi.org/10.1016/j.apradiso.2016.07.007
0969-8043/

optical fibers usually used in FOD, the luminescence due to Cherenkov effect is the main stem effect component. Cherenkov effect is generated during irradiation of the optical fiber, when electrons from outside get into the fiber core at speeds higher than the speed of light. These electrons decelerate and emit electromagnetic radiation having an intensity proportional to λ^{-3} (λ=wavelength). For this reason, stem effect is more important in the blue region of the visible spectrum (De Boer, 1993). The net contribution of stem effect depends not only on the position of the scintillator, but also on the length and position of the irradiated optical fiber with respect to the beam. For this reason, the stem effect must be reduced if a reliable estimation of the dose rate is required. Several techniques have been proposed to reduce or eliminate the stem effect. The first one consists in using a fiber with a scintillator next to a reference blank fiber having no detector. Thus the signal of the scintillator is obtained by subtracting the signal of the reference fiber from the signal of the fiber having the scintillator (Beddar et al., 1992a, 1992b). This technique reduces the spatial resolution of the detector. Another technique resorts to a fiber with a hollow air core (Lambert et al., 2008), which affects ruggedness and decreases light transmission from scintillator to detector. A third method relies on the spectral discrimination to separate the scintillator signal from the stem effect (Fontbonne et al., 2002; Guillot et al., 2011; Veronese et al., 2013). This technique, called chromatic method, is effective, although requiring a rather complex setup. A fourth method relies on the temporal discrimination of the RL signal from the stem emission. It consists in measuring the RL signal between pulses of a LINAC (Martinez et al., 2015). This technique, which only can be used in LINACs, requires that the scintillator has an afterglow longer than the duration of the LINAC pulse. Finally, using red-emitting scintillators as FOD detectors permits to reduce the Cherenkov contribution by using optical filters. This technique is easy to implement, cheap and optimizes optical coupling with Si-based light detectors (Clift et al., 2000).

In last years, several investigations led to the development and marketing of a FOD system called Exradin W1 Scintillator (Beierholm et al., 2014; Carrasco et. al, 2015a; Underwood et al., 2015). A number of debates related to the energy dependence of the Cerenkov light ratio (CLR) coefficient of the mentioned commercial system have been reported (Beierholm et al., 2015; Carrasco et al., 2015b). The CLR coefficient takes into account the contribution of the stem effect to the total measured signal and some uncertainty related to the temporal change in CLR seems to be related to accumulated dose in Exradin W1 (Beierholm et al., 2015). In particular, Beierholm et al. recommend "that users of the W1 consider how the calibration coefficients of their detector change with beam quality and accumulated dose" in order "to minimize uncertainties associated with the use of the Exradin W1 scintillator". On the other hand, Carrasco et al. conclude that "further studies using different W1 are required to conclude whether the manufacturer should provide these detectors with a preirradiation dose high enough to stabilize them" and "further studies will be key to reduce the uncertainties related to CLR and gain determination during the calibration procedure. Without this reduction, we cannot conclude that it shows any energy dependence in the studied range" (Carrasco et al., 2015b).

Several red-emitting phosphors have been studied as FOD detectors so far. For instance, $Li_2B_4O_7$(Mn)-based FOD probes demonstrated to have a response similar to soft tissue and emission at 600 nm related to Mn-centres has been observed (Santiago et al., 2009). BC-430 red emitting plastic scintillator has been also investigated as a possible tissue equivalent FOD detector, which provides increased signal when coupled to a photodiode (Clift et al., 2000). Perovskite $KMgF_3$(Sm) crystals also show emission in the red spectral region due to characteristic radiative transitions of Sm^{2+} and Sm^{3+} cations (Marcazzó et al., 2010). Similar investigations have been carried out by Veronese et al. (2014) by using Yb-doped fibers which emits in the infrared region for real time ionizing radiation detection.

Recent studies have demonstrated the feasibility of using Y_2O_3:Eu^{3+}, Y_2O_2S:Eu^{3+} and YVO_4: Eu^{+3} phosphors as red-emitting scintillators in the framework of the FOD technique (Molina et al., 2013). The high RL efficiency of these phosphors in the red spectral region allows to use simple optical filtering methods to reduce the spurious luminescence caused by the stem effect. Although the mentioned phosphors are not tissue equivalent, they perform very well as compared to an ion-chamber to acquire a percentage depth dose profile in a water phantom if the field size is smaller than 3×3 cm^2 (Martinez et al., 2015). The aforementioned Eu-doped Yttrium-based phosphors were originally meant as efficient red-emitters for CRT screens and are commercially available. The industry has developed a variety of red-emitting phosphors for different purposes. Red-emitting scintillators having different optical properties have been fabricated for ionizing particle detection in nuclear physics, which could be suitable to be employed as FOD detectors. Among them, ZnSe(Te) appears as a scintillator that could fit the requirements of a FOD detector. ZnSe: Te crystals are non-higroscopic and show quick stability of its scintillation. In particular, optical transitions in ZnSe(Te) result in luminescence band peaked at 600–630 nm, which is convenient for subsequent detection by conventional photodetectors (Ryzhikov et al., 2003). However, its effective atomic number is higher than water (Zeff=33), which could affects its applicability as dosimeter to irradiation conditions when low energy photons are present (Martinez et al., 2015).

In this work a ZnSe(Te)-based FOD probe has been built and its response under irradiation in conditions similar to those found in radiotherapy has been investigated. In particular the performance of optical filtering for reducing the stem effect contribution in this red-emitting scintillator has been assessed. Furthermore, reproducibility of the probe has been studied and the minimum detectable dose rate calculated. Finally, the response of the ZnSe (Te)-based FOD probe has been compared to that of an ion-chamber to obtain percent depth dose (PDD) curves in a LINAC facility in different irradiation field sizes.

2. Materials and methods

In the present work ZnSe(Te) cylinders of 1 mm diameter and 2 mm length from Moltech GMBH (Germany) were employed. In order to build the FOD probes an Eska™ PMMA optical fiber (1 mm core diameter, 10 m length) was used. A ZnSe(Te) cylinder was glued to one end of the optical fiber by using UV-curing Norland 68 adhesive (Norland Products Incorporated, NJ, USA) and eventually covered with a layer of opaque paint. The other fiber end was terminated with a SMA connector. In order to evaluate the contribution of the stem effect, a dummy FOD probe was fabricated consisting in a 10 m length optical fiber having no detector at its end.

In order to determine the RL spectrum of the commercial ZnSe (Te) crystals a naked sample was irradiated at room temperature (RT) with a 3.7×10^8 Bq ophthalmic 90 Sr beta-source rendering a dose rate of 0.022 Gy/min at the sample position. The spectrum of the emitted light was recorded by means of an Acton Research SP-2155 0.150 m monochromator featuring a Hamamatsu H9319 photon counting PMT having sensitivity between 300 and 850 nm. The spectrum was measured within the 300–800 nm wavelength range at a rate of 20 nm/min. The sample was placed at the entrance slit and irradiated with the aforementioned beta-source, which was situated 1 cm away from the sample. A resolution of

approximately 5 nm was obtained by setting the entrance and exit slits width at 3 mm during the measurements. The RL spectrum of the FOD probe was determined in a Theratron 80 Cobalt-60 facility with a dose rate of 0.35 Gy/min at 5 mm depth in water, 80 cm Source-Surface distance (SSD) and 10×10 cm^2 field size. The fiber end having attached the ZnSe(Te) crystal was positioned at the center of the radiation field at 5 cm water depth. The optical fiber was oriented horizontally and parallel to one of the field sides. Under these conditions, approximately 5 cm of the optical fiber was directly exposed to primary radiation beam. The aforementioned monochromator and light detector were employed for the spectrum measurement. The FOD probe was directly connected to the input slit of the monochromator via the SMA termination.

In order to investigate the behavior of the ZnSe(Te) RL signal as a function of irradiation time, irradiations in two different facilities were carried out. In LINAC, the ZnSe(Te)-based FOD probe was irradiated at two different dose rates by using a 6 MV Varian LINAC. Measurement were performed in water at SSD constant (100 cm) and at 14 mm (dose rate=1.28 Gy/min) and 84,7 mm depth (dose rate=0.77 Gy/min) in a 1×1 cm^2 size field. In Cobalt-60 facility, measurements were carried out in air by resorting to a Theratron 80, at a 10×10 cm^2 size field, with source-detector distance (SDD) of 80 cm (dose rate=0.374 Gy/min) by using a build-up cap for ensuring electronic equilibrium. The probe was placed in the central point of the field. Several consecutives exposures varying irradiation interval and time between successive expositions were measured. In both, LINAC and Cobalt-60 facility, probe was directly connected to a Hamamatsu H9319 photon counting head via a SMA connector.

Percent Depth Dose (PDD) curves were obtained with the FOD probe in order to determine the conditions under which the probe could perform as a tissue-equivalent detector, say, without needing further correction of its lecture. PDD curves represent the percentage of dose deposited in water at different depths, with respect to the point of maximum dose. The PDD curves were thus compared with PDD curves obtained in the same conditions with a PTW pinpoint ion-chamber in a LINAC facility. In a 6 MV LINAC this point is located around 15 mm depth (10×10 cm^2 field size) and its position shifts to lower depths as the field size goes below 4×4 cm^2 (Sixel and Podgorsak, 1994). PDD curves were obtained in a Varian 6 MV X-ray LINAC at 100 cm Source-Surface distance (SSD) with different field sizes, namely, 1×1, 3×3, 5×5 and 10×10 cm^2. These measurements were made using a Civco MT-100 water phantom with manual vertical positioning (accuracy 0.1 mm). The light yield of the FOD probe was measured by using the same Hamamatsu photon counting head mentioned above. Long-pass coloured glass filters were employed in order to minimize the stem effect during in situ measurements. In particular, a 3 mm thick Schott OG610 filter having cut-off wavelengths at 610 nm was used. For comparison PDD profiles were obtained in identical conditions with a PinPoint ion-chamber (PTW 31,014, PTW UNIDOS E electrometer).

3. Results and discussion

In Fig. 1 the RL spectrum of a bare ZnSe(Te) crystal as function of photon energy is shown. The spectrum has been corrected for the spectral response of the spectrometer and the light detector. As can be seen from the figure, the spectrum is dominated by a broad emission band having peak at 1.98 eV (626 nm). This band presents a subtle shoulder on the low energy side, which is an evidence that the observed band is composite actually. Although a detailed study of the processes that take place during the RL emission of ZnSe(Te) is beyond the aim of this work, a brief description can be given by taking into account the existing literature

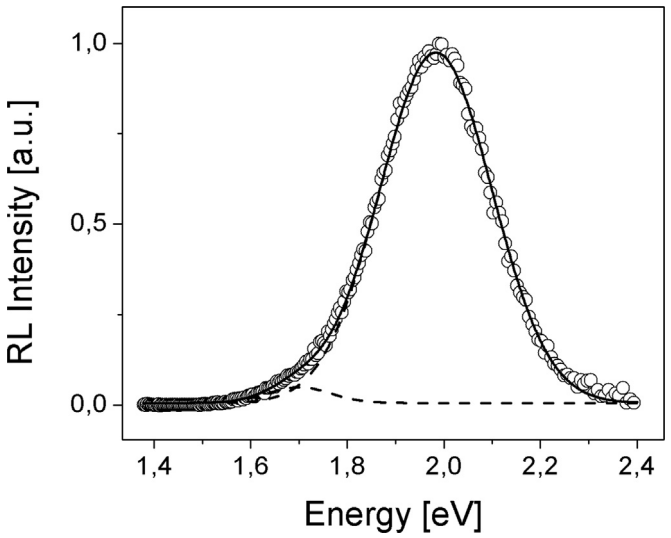

Fig. 1. RL emission spectrum of a bare ZnSe(Te) crystal (open circle). The curve has been fitted by two fitted Gaussians curves (dash line). The black solid line is the sum of the Gaussians components.

dealing with the scintillation properties of this material. ZnSe(Te) luminescence spectrum is found to be strongly dependent on thermal treatment in different environments during fabrication (Ryzhikov et al., 2003). Competition between radiative and non-radiative recombination paths results in two strongly overlapping emission bands centered at 635 nm and 463 nm (Ryzhikov, 2001). In some cases, a narrow band peaking at 708 nm has been also detected (Kolesnikov et al., 2014). In our case, only the band at 626 nm is observed. Regarding this band, Makhni and Tkachenko (2003) have found that it results from the contribution of three different donor-acceptor-type transitions depending their relative intensity on the ratio between Zn vacancies and Te concentrations finally achieved after crystal growth. Two of these transitions result in emission at 1.95 eV (~630 nm) and 1.9 (~650 nm), being responsible the third one for emission at 1.7 eV (~730 nm). In our case, it seems that the three mentioned transitions contribute to make up the observed RL emission band, being the transition at 1.7 eV responsible for the subtle shoulder observed at lower energy. In fact, two gaussian curves can be fitted to the curve shown in Fig. 1 having maxima at 1.98 eV and 1.7 eV respectively (see Table 1). In principle the transitions at 1.95 and 1.9 eV as reported by Makhni and Tkachenko could be responsible for the fitting peak centered at 1.98 eV observed in the RL spectrum of the commercial ZnSe(Te) crystal employed in the present work. The fitting component peaking at 1.7 eV clearly corresponds to the peak at the same energy by Makhni and Tkachenko (2003).

In Fig. 2 the RL spectrum of the ZnSe(Te)-based FOD probe irradiated in the Cobalt-60 facility is shown. As before, the RL spectrum was not corrected for the spectral response of the system, namely, by the quantum efficiency of the optical detector and optical fiber attenuation. Curve (a) corresponds to the dummy probe (optical fiber without ZnSe(Te) detector). This spectrum is more intense in the blue region and decreases as the wavelengths

Table 1
Fitting parameters resulting from the fit of two Gaussian curves to the spectrum curve shown in Fig. 1 (R^2=0.998).

Peak #	Energy [eV]	FWHM [eV]	Relative integrated area [%]	Relative intensity [%]
1	1,700 ± 0,003	0,130 ± 0,006	2,4 ± 0,2	4,5 ± 0,1
2	1,9835 ± 0,0002	0,2328 ± 0,0005	97,6 ± 0,2	100

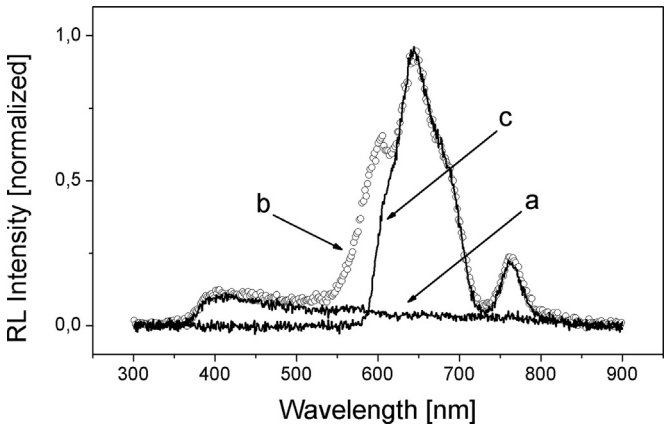

Fig. 2. RL emission spectrum of dosimetric system dummy end (a), ZnSe(Te) detector end (b) and ZnSe(Te) detector end using 610 nm filter in the system (c).

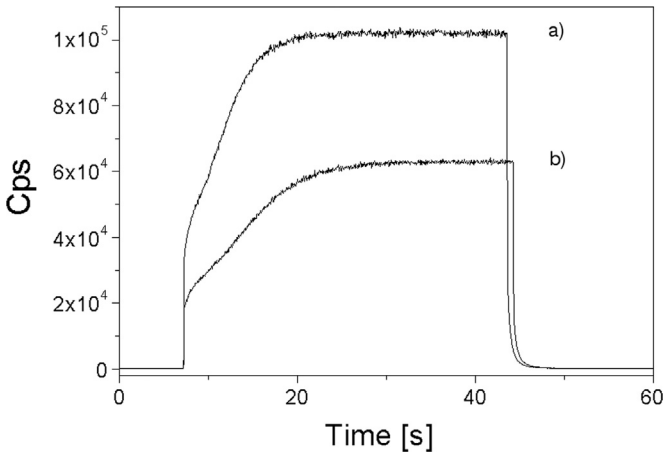

Fig. 3. ZnSe(Te) RL curve during irradiation in LINAC at different dose rates: (a) 1.28 Gy/min, (b) 0.77 Gy/min.

increases, as expected for stem effect (Molina et al., 2012). Curve (b) corresponds to the spectrum of the ZnSe(Te)-based FOD probe. Between 500 and 800 nm expected emission of ZnSe(Te) is observed (Makhni and Tkachenko, 2003), which adds to the stem effect contribution. I we compare the curve shown in Fig. 2(b) with that in Fig. 1, it is clear that two dips appear at 600 and 740 nm respectively. In both cases they can be attributed to characteristic attenuation maxima of the ESKA PMMA optical fiber employed to fabricate the dosimetry probe (Industrial Fiber Optics, 2016), which modulates the RL emitted by the ZnSe(Te) crystal attached to the optical fiber end. In order to reduce the stem effect contribution the RL signal has been optically filtered by means of a 610 nm cut-off long-pass filter (Schott RG 610). The resulting spectrum can be observed in Fig. 2 (curve(c)). If the RL signal is recorded without using any filter, the integrated contribution of the stem effect amounts to 12% of the total RL integrated signal. On the other hand, if the long-pass filter is employed the stem effect contribution goes down to 1.2% of the total RL signal. If we assume that most of the stem effect light is produced within the 5 cm of the optical fiber directly exposed to the primary radiation beam, the percentage stem effect contribution per unit length remaining after optical filtering amounts to 0.24% per centimeter. This value could be pointed out as a rough estimate of the efficiency of the optical filtering method to reduce the stem effect contribution in the particular conditions of the present work.

Although the stem effect contribution cannot be eliminated, the reduction is higher than that reported by Clift (Clift et al., 2000) when filtering the emission of a red-emitting BC-430 plastic scintillator. In their work Clift et al. report 3% stem effect reduction by resorting to the combination of two band-pass coloured filters and the enhancement of scintillation light by coating the detector with reflecting layers. The higher scintillation efficiency of ZnSe (Te) relative to BC-430 and its emission centered at higher wavelength could be responsible of this result. In what follows, the RL signal coming from the FOD probe has been filtered with the mentioned long-pass optical filter.

In order to investigate the shape of the RL signal of ZnSe(Te) on irradiation time, the ZnSe(Te)-based FOD probe was irradiated at two different dose rates in LINAC (see Fig. 3), the first one at 1.28 Gy/min (curve a) and the second one at 0.77 Gy/min (curve b). The RL curve shows an initial region in which the signal rises up to the stabilization, where the scintillation yield is almost constant. From Fig. 3 it is possible to estimate in each case the saturation time, say, the time it takes for the signal to reach 95% of its maximum value. The saturation times amounts to 13 s (curve a) and 20 s (curve b). If translated to dose, both saturation times correspond to almost the same dose: 0.27 and 0.26 Gy respectively. Similar delay of the RL signal to reach a constant value has been also observed in other FOD materials (Al_2O_3: C, for instance). This effect could be related to the presence of shallow traps, which capture part of the free charges released by radiation (Damkjaer et al., 2008). The RL signal reaches a constant value once the trap filling rate becomes constant or traps saturate. In the case of Al_2O_3: C the stability under 6 MV X-ray irradiation is reached more than 200 s after irradiation begins, namely, approximately 20 Gy (Andersen et al., 2011).

In order to investigate whether the RL signal remains constant as dose increases, the behavior of the RL emission of the probe at different irradiation times in a Cobalt-60 facility has been investigated (Fig. 4). The irradiation time was increased (36.15, 72.30, 108.45, 144.60, 180.75, 217.50 and 290 s respectively) as the lapse between irradiations was kept constant (60 s). In all cases the RL signal reaches a saturation value, which is constant within each irradiation interval. Time to reach this value is approx. 50 s, which implies an accumulated dose of 0.275 Gy in agreement with the results shown in Fig. 3 as commented in previous paragraph.

The influence of the time elapsed between consecutive irradiations on the shape of the RL signal was also analyzed by using the same configuration described previously. In this case (see Fig. 5), irradiation time was kept constant but the time elapsed between irradiations (E_t) was increased (15, 40, 100, 200, 300, 400 and 600 s). In the inset of Fig. 5 the curves have been rearranged to start at the same instant in order to permit the comparison of the

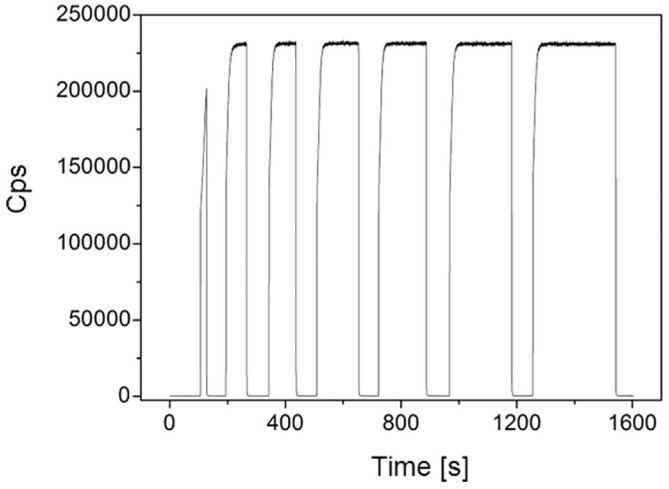

Fig. 4. RL emission during sequential measurements, with constant relaxation time.

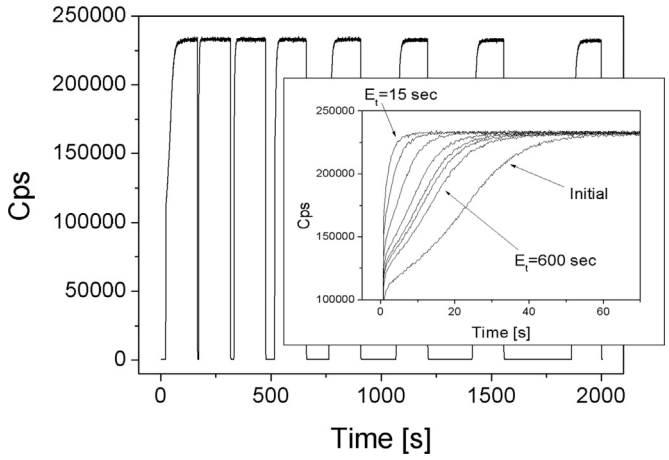

Fig. 5. Change of the initial portion of the RL emission during sequential measurements, varying the relaxation time. In the inset E_t stands for the time elapsed between successive irradiations.

initial portion of each curve. It is apparent from the figure that the raising time decreases with the time elapsed since the end of the previous irradiation. Even 600 s are not enough for the probe to recover the initial conditions. On the other hand, this result points out that a pre-irradiation procedure could be necessary in order to ensure a prompt response of the probe to the actual dose rate value (Andersen et al., 2011; Akino et al., 2015). In this context, if a pre-irradiation dose higher than 0.275 Gy is given to the ZnSe(Te) probe, a linear RL response in a dose range between 0.01 and 1 Gy was observed.

In order to determine the repeatability of RL signal of the ZnSe (Te) probe, it was irradiated eight consecutive times in the Co-60 facility in the same conditions described above. Both the irradiation and relaxation time were kept constant and equal to 100 s. In Fig. 6 the average of the RL signal computed from of the last ten seconds of each irradiation interval is shown. The RL response values were normalized to the value obtained for the first irradiation. The error bars correspond to the normalized standard deviations of each average. Although a drift of the RL signal seems to be present, the signal change is within the value of the error bars and well below 0.5%. The minimum detectable dose rate has been estimated as usually by taking into account the standard deviation of the background signal (Martinez et al., 2015). The procedure consists in measuring several times the signal yield

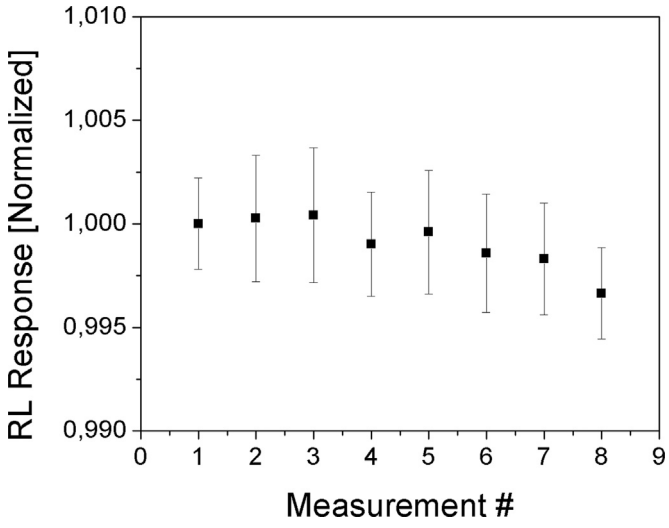

Fig. 6. RL response of the ZnSe(Te) detector after eight consecutive measurement.

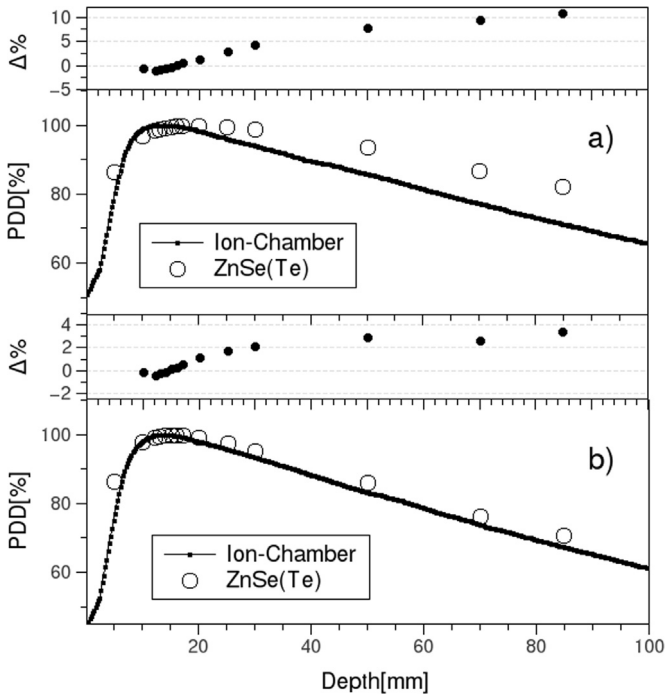

Fig. 7. PDD curves recorded with the ZnSe(Te) probe (circles) and the ion-chamber (line): (a) 10×10 and (b) 5×5 cm^2 field size.

obtained when the probe is not being irradiated, namely, the dark current, to obtain the average and standard deviation of measurement set. Then the lowest detection limit is determined as the dose rate equivalent to four times the standard deviation. In this work, the dark current brought about 55 ± 8 cps. As for our configuration 10^5 cps corresponds to a dose rate of 1.28 Gy/m (see Fig. 3), then the minimum detectable dose rate amounts to 0.41 mGy/m.

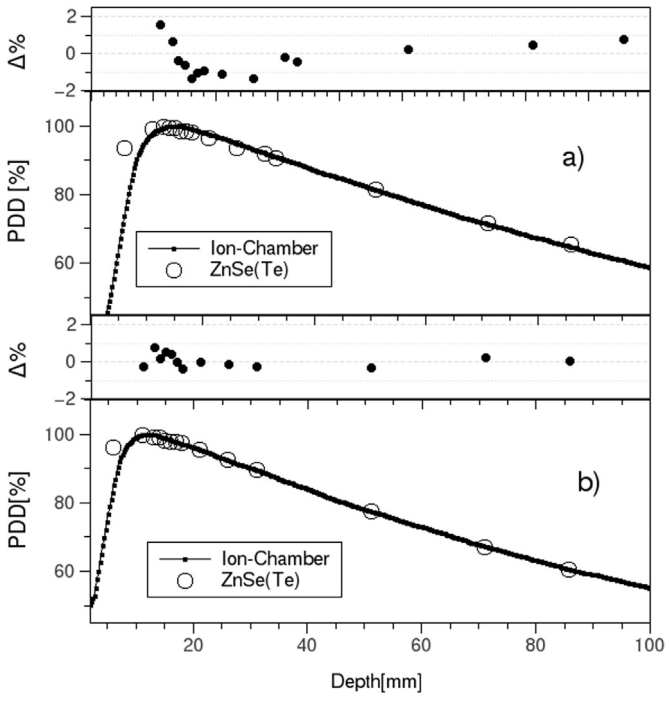

Fig. 8. PDD curves recorded with the ZnSe(Te) probe (circles) and the ion-chamber (line): (a) 1×1 cm^2 and (b) 3×3 cm^2 field size.

In Figs. 7 and 8, the PDD curves recorded with the ZnSe(Te) detector for different field sizes are compared with PDD curves from ion-chamber irradiated in the LINAC at 6 MV. Fig. 7 corresponds to results obtained with 10×10 and 5×5 cm^2 field sizes. Fig. 8 shows results for smaller field sizes, namely, 3×3 and 1×1 cm^2, respectively. The value of the RL signal after saturation (see Fig. 3) has been considered in each case to determine the PDD plots. In each case the percentage difference (%) between both curves is shown.

In 10×10 cm^2 field (see Fig. 7) the PDD curve of the ZnSe(Te) probe does not present a maximum point of yield at the expected depth (15 mm). It shows instead a rounded peak having maximum at a deeper position with respect to the ion-chamber. Furthermore, an over response with respect to the ion-chamber is apparent at higher depths. In the same figure, as the field size reduces to 5×5 cm^2 the difference becomes less important. In fact, the peak at 15 mm depth is clearly defined and a lower over response ($< 4\%$) is observed as the depth increases.

On the other hand, in small fields (Fig. 8) the PPD curve obtained with the ZnSe(Te) probe matches that of the pin-point ion-chamber (within a range of 1%), except in the build-up region. This effect could be related to the volume effect, since the diameter of the ZnSe(Te) detector is about 1 mm and the diameter of the pin-point ionization chamber is 2 mm (Laub and Wong, 2003). A loss of charge particle equilibrium in this region could also be responsible for the observed difference.

The behavior of the observed PDD curves could be explained by taking into account that for ZnSe(Te) the effective atomic number is $Z_{eff}=33$, which is higher than that of water ($Z_{eff}=7.4$). This fact results in an over response of ZnSe(Te) with respect to water due to the low energy photons present in secondary radiation. Since secondary radiation production increases as the field size grows, more important differences between the FOD probe and the ion-chamber could be expected in large field sizes. According to the results obtained in Fig. 8, the response of the ZnSe(Te)-based FOD probe is similar to that of the ion-chamber for field sizes smaller than 5×5 cm^2 at 6 MV photon energies.

4. Conclusions

In this work, performance of red-emitting ZnSe(Te) scintillator as fiber optic dosimeter detector has been studied for the first time. In this context, a percent depth dose study of this probe was compared to that of an ion-chamber in the LINAC facility and a very good response of this probe in small fields was observed. A good reproducibility of the RL response with a percent standard deviation lesser than 0.5% was obtained. The minimum detectable dose of the ZnSe(Te) probe has been estimated to be 0.41 mGy/m.

Optical filtering of the RL signal has been employed to reduce the stem effect contribution from 12% up to 1.2% of the total RL signal. Although further research is required in order to determine the feasibility of using this material as a FOD detector, results presented in this work demonstrate prospects for further research of ZnSe(Te)-based fiberoptic probes.

Acknowledgements

We acknowledge the financial support received from PICT 2012-0715 and 2015-2647 (ANPCyT, Argentina) and PIPs 1076/2012 and 800/2015 (CONICET, Argentina). We are grateful to Dr. W. Ponce and Bioeng. Soledad Machello (Centro Oncológico de la Sierra, Tandil, Argentina) for their valuable assistance to perform the measurements at the LINAC facility.

References

Akino, Y., Gautam, A., Coutinho, L., Würfel, J., Das, I., 2015. Characterization of a new commercial single crystal diamond detector for photon and proton-beam dosimetry. J. Radiat. Res., 1–7.

Andersen, C.E., Damkjær, S.M.S., Kertzscher, G., Greilich, S., Aznar, M.C., 2011. Fiber-coupled radioluminescence dosimetry with Saturated Al2O3: C Crystals: Characterization in 6 and 18 MV Photon beams. Rad. Meas. 46, 1090–1098.

Aznar, M.C., Andersen, C.E., Bøtter-Jensen, L., Bäck, S.A.J., Mattsson, S., Kjær-Kristoffersen, F., Medin, J., 2004. Real-time optical-fibre luminescence dosimetry for radiotherapy: physical characteristics and applications in photon beams. Phys. Med. Biol. 49, 1655–1669.

Beddar, A.S., Mackie, T.R., Attix, F.H., 1992a. Cerenkov light generated in optical fibres and other light pipes irradiated by electron beams. Phys. Med. Biol. 37 (4), 925–932.

Beddar, A.S., Mackie, T.R., Attix, F.H., 1992b. Water-equivalent plastic scintillation detectors for high energy beam dosimetry: I. Physical characteristics and theoretical considerations. Phys. Med. Biol. 37, 1883–1900.

Beierholm, A.R., Behrens, C.F., Andersen, C.E., 2014. Dosimetric characterization of the Exradin W1 plastic scintillator detector through comparison with an in-house developed scintillator system. Radiat. Meas. 69, 50–56.

Beierholm, A.R., Behrens, C.F., Andersen, C.E., 2015. Comment on characterization of the exradin W1 scintillator for use in radiotherapy. Med. Phys. 42, 4414–4416 [Med. Phys. 42, 297–304 (2015)].

Beierholm, A.R., Ottosson, R.O., Lindvold, L.R., Behrens, C.F., Andersen, C.E., 2011. Characterizing a pulse-resolved dosimetry system for complex radiotherapy beams using organic scintillators. Phys. Med. Biol. 56, 3033–3045.

Beierholm, A.R., Damkjær, S.M.S., Behrens, C.F., Andersen C.E., 2012. Approaching pulse-resolved, non-perturbing dose verification of dynamic radiotherapy, European Society for Radiotherapy & Oncology ESTRO 2012, OC-0226, pp. S88–S89.

Caraca Santos, A., Mohammadi, Mohammad, Shahraam, Afshar V., 2015. Evaluation of a real-time BeO ceramic fiber-coupled luminescence dosimetry system for dose verification of high dose rate brachytherapy. Med. Phys. 42, 6349.

Carrasco, P., Jornet, N., Jordi, O., Lizondo, M., Latorre-Musoll, A., Eudaldo, T., Ruiz, A., Ribas, M., 2015a. Characterization of the Exradin W1 scintillator for use in radiotherapy. Med. Phys. 42, 297–304.

Carrasco, P., Jornet, N., Jordi, O., Lizondo, M., Latorre-Musoll, A., Eudaldo, T., Ruiz, A., Ribas, M., 2015b. Response to Comment on 'Characterization of the Exradin W1 scintillator for use in radiotherapy'. MEd. Phys. 42, 44147–44418 [MEd. Phys. 42, 297–304 (2015)].

Clift, M.A., Sutton, R.A., Webb, D.V., 2000. Dealing with Cerenkov radiation generated in organic scintillator dosimeters by bremsstrahlung beams. Phys. Me. Biol. 45, 1165–1182.

Damkjaer, S., Andersen, C.E., Aznar, M.C., 2008. Improved real-time dosimetry using the radioluminescence signal from Al2O3: C. Radiat. Meas. 43, 893–897.

De Boer, S.F., Beddar, A.S., Rawlinson, J.A., 1993. Optical filtering and spectral measurements of radiation-induced light in plastic scintillation dosimetry. Phys. Med. Biol. vol. 38, 945–958.

Fontbonne, J.M., Iltis, G., Ban, G., Battala, A., Vernhes, J.C., Tillier, J., Bellaize, N., Le Brun, C., Tamain, B., Mercier, K., Motin, J.C., 2002. Scintillating Fiber Dosimeter for Radiation Therapy Accelerator. IEEE Trans. Nucl. Sci. Vol 49, 2223–2227.

Guillot, M., Gingras, L., Archambault, L., Beddar, S., Beaulieu, L., 2011. Spectral method for the correction of the Cerenkov light effect in plastic scintillation detectors: a comparison study of calibration procedures and validation in Cerenkov light-dominated situations. Med. Phys. 38, 2140–2150.

Huston, A.L., Justus, B.L., Falkenstein, P.L., Miller, R.W., Ning, H., Altemus, R., 2001. Remote optical fibre dosimetry. Nucl. Instrum. Methods Phys. Res. B 184, 55–67.

Industrial Fiber Optics, ESKA PMMA data sheet, URL: ⟨http://i-fiberoptics.com/pdf/attenuation.pdf⟩, April 1st, 2016.

Justus, B.L., Falkenstein, P.L., Huston, A.L., 2004. Gated fiber-optic-coupled detector for in vivo real-time radiation dosimetry. Appl. Opt. 43, 1663.

Kolesnikov, N.N., Borisenko, E.B., Borisenko, D.N., Zverkova, I.I., Tereshchenko, A.N., Timonina, A.V., Gnesin, I.B., Gartman, V.K., 2014. Ceramic material ZnSe(Te) fabricated by nanopowder technology: Fabrication, phase transformations and photoluminescence. J. Cryst. Growth 401, 849–852.

Lambert, J., Yin, Y., McKenzie, D.R., Law, S., Suchowerska, N., 2008. Cerenkov free scintillation dosimetry in external beam radiotherapy with an air core light guide. Phys. Med. Biol. 53, 3071–3080.

Lambert, J., Yin, Y., McKenzie, D.R., Law, S.H., Ralston, A., Suchowerska, N., 2010. A prototype scintillation dosimeter customized for small and dynamic megavoltage radiation fields. Phys. Med. Biol. 55 (4), 1115–1126.

Laub, W.U., Wong, T., 2003. The volume effect of detectors in the dosimetry of small fields used in IMRT. Med. Phys. 30 (3), 341–347.

Létourneau, D., Pouliot, J., Roy, R., 1999. Miniature scintillating detector for small field radiation therapy. Med. Phys. 26 (12), 2555–2561.

Makhni, V., Tkachenko, I., 2003. Mechanism for forming the red emission band of ZnSe < Te > scintillation crystals. Opt. Zhurnal 70, 54–57 (Ukraine).

Marcazzó, J., Santiago, M., D'Angelo, C., Furetta, C., Caselli, E., 2010. Study of the luminescent properties of KmgF3: Sm. Nucl. Instrum. Methods Phys. Res. Sect. B: Beam Interact. Mater. At. 268, 183–186.

Martinez, N., Teichmann, T., Molina, P., Sommer, M., Santiago, M., Henniger, J., Caselli, E., 2015. Scintillation properties of the YVO4: Eu3+ compound in powder form: its application to dosimetry in radiation fields produced by pulsed mega-voltage photon beams. Z. Med. Phys. 25, 368–374.

Molina, P., Sommer, M., Kattner, F., Henniger, J., 2013. Response characterization of an Y2O3: Eu-based radioluminescence probe under 60Co irradiation. Rad. Meas. 56, 338–341, ISSN 1350-4487.

Molina, P., Santiago, M., Marcazzó, J., Spano, F., Henniger, J., Cravero, W., Caselli, E., 2012. Radioluminescence of red-emitting Eu-doped phosphors for fiberoptic dosimetry. Appl. Radiat. Isot. 71 (2012), 12–14.

Polf, J.C., Yukihara, E.G., Akselrod, M.S., y McKeever, S.W.S., 2004. Real-time luminescence from Al_2O_3: C fiber dosimeters. Rad. Meas. 38, 227–240.

Ryzhikov, V., Starzhinskiy, N., Galchinetskii, L., Silin, V., Tamulaitis, G., Lisetskaya, E., 2001. The role of oxygen in formation of radiative recombination centers in $ZnSe_{1-x}Te_x$ crystals. Int. J. Inorg. Mater. 3, 1227–1229.

Ryzhikov, V., Tamulaitis, G., Starzhinskiy, N., Galchinetskii, L., Novickovas, A., Kazlauskas, K., 2003. Luminescence dynamics in ZnSeTe scintillators. J. Lumin. 101, 45–53.

Santiago M., Prokic M., Molina P., Marcazzó J., Caselli E., 2009. A Tissue-Equivalent Radioluminescent Fiberoptic Probe for In-Vivo Dosimetry Based on Mn-Doped Lithium Tetraborate. IFMBE Proceedings 25/III, pp. 367–70.

Seymour, E., Downes, S., Fogarty, G.B., Izard, M., Metcalfe, P., 2011. In vivo real-time dosimetric verification in high dose rate prostate brachytherapy. Med. Phys. 38, 4785–4794.

Sixel, K.E., Podgorsak, E.B., 1994. Buildup region and depth of dose maximum of megavoltage xray beams. Med. Phys. 21, 411–416.

Teichmann, T., Sponner, J., Jakobi Ch, Henniger, J., 2016. Real time dose rate measurements with fiber optic probes based on the RL and OSL of beryllium oxide. Radiat. Meas. . http://dx.doi.org/10.1016/j.radmeas.2016.01.015

Underwood, T.S.A., Rowland, B.C., Ferrand, R., Vieillevigne, L., 2015. Application of the Exradin W1 scintillator to determine Ediode 60017 and microDiamond 60019 correction factors for relative dosimetry within small MV and FFF fields. Phys. Med. Biol. 60, 6669–6683.

Veronese, I., De Mattia, C., Fasoli, M., Chiodini, N., Mones, E., Cantone, M.C., Vedda, A., 2014. Infrared luminescence for real time ionizing radiation detection. Appl. Phys. Lett. 105, 061103.

Veronese, I., Cantone, M.C., Catalano, M., Chiodini, N., Fasoli, M., Mancosu, P., Mones, E., Moretti, F., Scorsetti, M., Vedda, A., 2013. Study of the radioluminescence spectra of doped silica optical fibre dosimeters for stem effect removal. J. Phys. D: Appl. Phys. 46, 015101–015108.